Skeletal defects in *ringelschwanz* mutant mice reveal that Lrp6 is required for proper somitogenesis and osteogenesis

Chikara Kokubu[1,*,†], Ulrich Heinzmann[2,*], Tomoko Kokubu[1], Norio Sakai[3], Takuo Kubota[3], Masanobu Kawai[3], Matthias B. Wahl[1], Juan Galceran[4], Rudolf Grosschedl[4], Keiichi Ozono[3] and Kenji Imai[1,‡]

[1]Institute of Developmental Genetics, GSF-National Research Center for Environment and Health, Ingolstädter Landstrasse 1, 85764 Neuherberg, Germany
[2]Institute of Pathology, GSF-National Research Center for Environment and Health, Ingolstädter Landstrasse 1, 85764 Neuherberg, Germany
[3]Department of Developmental Medicine (Pediatrics), Osaka University Graduate School of Medicine, 2-2 Yamadaoka, Suita, Osaka 565-0871, Japan
[4]Gene Center and Institute of Biochemistry, Ludwig Maximilians University, Feodor Lynenstrasse 25, 81377 Munich, Germany
*These authors contributed equally to this work
[†]Present address: Department of Social and Environmental Medicine, Graduate School of Medicine, Osaka University, Suita, Osaka 565-0871, Japan
[‡]Author for correspondence (e-mail: imai@gsf.de)

Accepted 17 August 2004

Development 131, 5469-5480
Published by The Company of Biologists 2004
doi:10.1242/dev.01405

Summary

Here, we present evidence that Lrp6, a coreceptor for Wnt ligands, is required for the normal formation of somites and bones. By positional cloning, we demonstrate that a novel spontaneous mutation *ringelschwanz* (*rs*) in the mouse is caused by a point mutation in *Lrp6*, leading to an amino acid substitution of tryptophan for the evolutionarily conserved residue arginine at codon 886 (R886W). We show that *rs* is a hypomorphic *Lrp6* allele by a genetic complementation test with *Lrp6*-null mice, and that the mutated protein cannot efficiently transduce signals through the Wnt/β-catenin pathway. Homozygous *rs* mice, many of which are remarkably viable, exhibit a combination of multiple Wnt-deficient phenotypes, including dysmorphologies of the axial skeleton, digits and the neural tube. The establishment of the anteroposterior somite compartments, the epithelialization of nascent somites, and the formation of segment borders are disturbed in *rs* mutants, leading to a characteristic form of vertebral malformations, similar to dysmorphologies in individuals suffering from spondylocostal dysostosis. Marker expression study suggests that Lrp6 is required for the crosstalk between the Wnt and notch-delta signaling pathways during somitogenesis. Furthermore, the Lrp6 dysfunction in *rs* leads to delayed ossification at birth and to a low bone mass phenotype in adults. Together, we propose that *Lrp6* is one of the key genetic components for the pathogenesis of vertebral segmentation defects and of osteoporosis in humans.

Key words: Lrp6, Wnt signaling, Somitogenesis, Osteoporosis, Mouse

Introduction

Two closely related single-pass transmembrane proteins Lrp5 and Lrp6 (Brown et al., 1998; Hey et al., 1998) comprise a subfamily of low-density lipoprotein (LDL) receptor-related proteins with diverse functional roles as cell-surface receptors (Nykjaer and Willnow, 2002; Strickland et al., 2002). Previous studies have shown that Lrp5 and Lrp6 function as coreceptors for Wnt ligands (He et al., 2004; Pinson et al., 2000; Tamai et al., 2000; Wehrli et al., 2000; Zorn, 2001). Wnt signaling plays important roles in a wide variety of biological processes during pre- and postnatal life in invertebrates and vertebrates. Downstream of the surface receptors, Wnt signaling is transduced through the so-called canonical pathway, which is dependent on β-catenin, or through other noncanonical pathways. A line of evidence supports that Lrp5/6 mediates only the canonical Wnt/β-catenin signaling pathway (Bafico et al., 2001; Mao et al., 2001a; McEwen and Peifer, 2001; Semenov et al., 2001; Wehrli et al., 2000). In the current model of the canonical Wnt/β-catenin signaling pathway, Wnt ligands bind to the frizzled receptor and form a ternary complex with Lrp5 or Lrp6 on the cell surface. This heterotrimeric complex formation results in the stabilization of β-catenin by inactivating the β-catenin destruction complex in the cytoplasm, which is a large multiprotein complex consisting of glycogen synthase kinase 3β (GSK3β), the tumor suppressor protein APC, the scaffold protein axin and several other proteins. In the absence of Wnt signaling, GSK3β phosphorylates β-catenin, leading to the ubiquitin-mediated degradation of β-catenin by the proteasome. Direct interaction between Lrp5/6 and axin, which is dependent on the Wnt-frizzled interaction, is thought to be important for the inactivation of GSK3β (Mao et al., 2001b). Upon Wnt signaling, stabilized β-catenin translocates into the nucleus and forms a complex with HMG-box containing transcription factors of the TCF/LEF1 family, leading to the activation of Wnt-target genes.

The Wnt pathway has recently been implicated in the control

of somitogenesis (Aulehla et al., 2003; Hamblet et al., 2002) and of bone mass in adults in humans and mice (Boyden et al., 2002; Gong et al., 2001; Kato et al., 2002; Little et al., 2002). In the context of somite development, Wnt signaling mediated by Wnt3a has been implicated in the specification and propagation of progenitor cells of the paraxial mesoderm in the primitive streak or in the tail bud (Takada et al., 1994; Yoshikawa et al., 1997), and this Wnt signaling is transduced through the canonical β-catenin signaling pathway (Galceran et al., 1999; Galceran et al., 2001). As late functions, Wnt signaling is also known to play essential roles in the dorso-ventral patterning of formed somites, which is required for proper development of the dermomyotome and the myotome (Capdevila et al., 1998; Fan et al., 1997; Münsterberg et al., 1995; Wagner et al., 2000). However, whether Wnt signaling plays any significant role in the periodic morphogenetic movement of somitogenesis that takes place in the presomitic mesoderm (PSM) had not been clear until recently. Mouse dishevelled 2 (*Dvl2*), together with its paralog dishevelled 1 (*Dvl1*), has recently been shown to be required for somite segmentation, through the analysis of *Dvl2*-single and *Dvl1;Dvl2*-double knockout mice (Hamblet et al., 2002). Furthermore, it has recently been demonstrated that a paralog of *Axin*, *Axin2* (also called conductin) exhibits a dynamic and cyclic expression profile in the PSM. This finding, together with the detailed analysis of the notch-delta signaling activity in *Wnt3a* mutants, has provided clear evidence for the involvement of Wnt signaling in the process of somitogenesis in the PSM, functioning upstream of notch-delta signaling (Aulehla et al., 2003). On the other hand, recent studies have also elucidated another, unexpected functional aspect of Wnt signaling in the postnatal life, with the identification of Lrp5 as one of the key genetic factors that control bone mass. Positional cloning of the gene responsible for osteoporosis-pseudoglioma syndrome (OPPG), an autosomal recessive disorder in humans, revealed that loss-of-function mutations in *LRP5* lead to a low bone mass phenotype (osteoporosis) (Gong et al., 2001).

Despite the availability of Lrp6-null mouse mutants (Pinson et al., 2000), whether Lrp6 plays any roles in somitogenesis during development and in the control of bone mass during adult life has not been known, because of strong pleiotropic effects of Lrp6 deficiency that leads to neonatal lethality (Pinson et al., 2000). In the present study, we demonstrate that Lrp6 is required for somitogenesis and osteogenesis, through the analysis of a novel spontaneous mouse mutation *ringelschwanz* (*rs*), identified in this study as a viable hypomorphic allele of *Lrp6*.

Materials and methods

Mice

The *rs* mutant strain is maintained on the BALB/c background. For a backcross mapping study, C57BL/6 mice were used as mating partners. For genetic complementation test, a *Lrp6*-null mutant strain, $Lrp6^{Gt(pGT1.8TM)187Wcs}$ (Pinson et al., 2000) (kindly provided by W. C. Skarnes), was used.

Genotyping by PCR

Lrp6 genotyping was performed by PCR-based RFLP analysis as follows. A 456-bp including exon 12 of *Lrp6* was amplified by PCR with primers: 5′-TTTCCCAAAATAGGACTCAACCG-3′ (forward) and 5′-CCCCAGTTTCAACCTTTGGATTATAC-3′ (reverse), under the following condition: initial denaturing at 94°C for 4 minutes, followed by 40 cycles of 94°C/30 seconds, 60°C/45 seconds, 72°C/45 seconds, and final elongation at 72°C for 8 minutes. A single-nucleotide difference between *rs*-mutant and wild-type alleles was detected by digestion of the PCR products with *Hpa*II.

Skeletal preparations

Skeletons of E14 and newborn specimens were prepared by a double staining procedure with Alcian blue 8 GX (Sigma) and Alizarin red S (Sigma), according to the procedure described previously (Kessel et al., 1990).

Scanning electron microscopy and semi-thin histology

Embryos (E11.5) for semi-thin histology and for scanning electron microscopy (SEM) were fixed in 4% paraformaldehyde (PFA) and post-fixed in 2% OsO_4. For semi-thin histology, specimens were dehydrated and embedded in EPON 812 (Merck). Sections (1 μm) were made with a Reichert Ultracut E (Leica) and stained with 1% Toluidin Blue (Merck). For SEM, fixed samples were critical-point-dried with CO_2 and sputter-coated with platinum. Coated specimens were examined in a JSM-6300F (JEOL).

Whole-mount RNA in situ hybridization

Whole mount in situ hybridization was performed as described (Kokubu et al., 2003) using digoxigenin-labeled riboprobes. The following cDNA probes were used in this study: *Sox10* (Kuhlbrodt et al., 1998), *Mesp2* (Saga et al., 1997), *Uncx4.1* (Mansouri et al., 1997), *Tbx18* (Kraus et al., 2001), *Dll1* (Bettenhausen et al., 1995), paraxis (Burgess et al., 1995) and *Lfng* (Evrard et al., 1998).

Assay for the Wnt-β-catenin pathway in cultured fibroblasts

Primary fibroblasts were prepared from minced dorsal skin of newborn animals. Fibroblasts were grown at 37°C in Dulbecco's modified Eagle's medium containing 15% fetal calf serum. Transient transfection was performed with lipofectamine (Invitrogen) according to the manufacturer's protocol. A LEF-luciferase (LUC) reporter plasmid, containing seven multimerized LEF1-binding sites linked to fos promoter-LUC gene, was transfected alone or in combination with expression plasmids for LEF1, β-catenin or Wnt1 as described (Hsu et al., 1998). A Rous sarcoma virus-β-galactosidase control plasmid was included in each transfection experiment to control for the efficiency of transfection. Luciferase and β-galactosidase assays were performed as described (Hsu et al., 1998).

X-ray radiography and bone histology

For X-ray radiography and bone histology of adult mice (Fig. 10), radiographs of the cadavers were taken in a cabinet X-ray system (Hewlett-Packard). Subsequently, the specimens were fixed in 4% PFA, decalcified in EDTA, and embedded in paraffin. Sections (5 μm thickness) were stained with hematoxylin and eosin. For histology of non-decalcified bones (Fig. 9), the left limbs were separated and fixed in 4% PFA. The right limbs were used for skeletal preparation. PFA-fixed limbs were dehydrated and embedded in methylmethacrylate and sectioned (5 μm) on a motorized Minot microtome (Jung). Serial sections was stained either with Alcian blue at pH 1.0 or with Alizarin red followed by hematoxylin.

BrdU and TUNEL assays

BrdU incorporation and TUNEL assays were carried out on 7-μm serial frozen sections as previously described (Yashiro et al., 2004). Briefly, pregnant females were injected intraperitoneally with 50 mg/(kg body weight) of BrdU (Amersham) at E10.5. The embryos were recovered after 1 hour, and processed for frozen sectioning. The detection of BrdU was performed using the Cell Proliferation Kit (Amersham). TUNEL staining was performed using the Apoptosis

Detection Kit (Takara). Immunoreaction was visualized with diaminobenzidine (DAB), and the sections were observed without counterstaining.

Peripheral quantitative computed tomography (pQCT)

Computed tomography was performed with the XCT Research SA+ and its associated software version 5.40 (Stratec Medizintechnik). Metaphyseal pQCT scans of tibiae were performed to determine the cortical and trabecular volumetric BMD and cortical thickness. The scan was positioned in the metaphysis at a distance of 1.7 mm from the proximal end of the epiphysis. The trabecular bone region was defined by peel mode 2, using a threshold at 395 mg/cm^3. Student's *t*-test was used for statistical evaluations.

Results

ringelschwanz mutant mice and their dysmorphology phenotypes

ringelschwanz (*rs*) mutant animals were recognized in 1998 by their extremely short and coiled-shape tail (Fig. 1A) in a BALB/c colony maintained at the GSF Research Center, thus we named the mutation *ringelschwanz* (i.e. 'coiled tail' in German). The first identified animal (male) was crossed with wild-type BALB/c females, and subsequent intercrosses of F_1 animals, all of which appeared normal, confirmed a recessive mode of inheritance of the *rs* trait. Approximately one-third of homozygotes die within one week after birth for undefined reasons. *rs/rs* animals showed malformations in the vertebral column (Fig. 1C-H) and in the neural tube (Fig. 1I,J). Neural tube defects (NTDs) in *rs* mutants were recognized in about 70% of homozygotes, and most often appeared in the form of spina bifida occulta in the lumbo-sacral region (Fig. 1E). However, in some cases spina bifida aperta could also be seen (Fig. 1J). Occasionally, *rs* homozygotes exhibited oligodactyly with the fifth digit missing in one or more limbs (Fig. 1K). The vertebral malformations in *rs* were strongest in the lumbo-sacral-tail region, while cervical and thoracic vertebrae appear fairly normal, except for frequent fusions between ribs at the proximal part (arrowheads in Fig. 1C-E). In the lumbo-sacral region of homozygotes, vertebral bodies were laterally split, or they sometimes fused to adjacent segments (Fig. 1C,H). Neural arches in the same region were also strongly malformed, such that both the ventral (pedicles) and dorsal (laminae) structures were often fused (Fig. 1D-F,H). Pedicles were occasionally not formed (yellow arrowheads in Fig. 1H). During embryonic development, the gross morphology of somites in *rs* mutants appeared fairly normal in the rostral part of embryos up to the lower thoracic region. However, from the lumbar region onwards, somites progressively became abnormal in shape, and somitogenesis was usually terminated when somitic tissues corresponding to around the tenth tail somites were generated.

Histological analysis of E11.5 embryos showed that somite segmentation in the lumbo-sacral region of *rs* mutant embryos was defective, and that somite borders became progressively unclear in a rostral-to-caudal direction (Fig. 2D,E compared to Fig. 2A,B, respectively). On parasagittal sections (Fig. 2B,E), the disruption of the segmental structure of dorsal root ganglia (DRGs) as fusion between DRGs was clearly observed in *rs*, suggesting that the somite AP polarity was impaired in *rs* mutants. On transverse sections, a reduction in the number of paraxial mesoderm cell was evident in *rs/rs*. The morphology of the neural tube was altered with an extended central channel in the dorsal region (Fig. 2F). The epithelial morphology of the dermomyotome (Fig. 2C) as well as that of nascent somites was not observed. Taken together, both the segmentation and

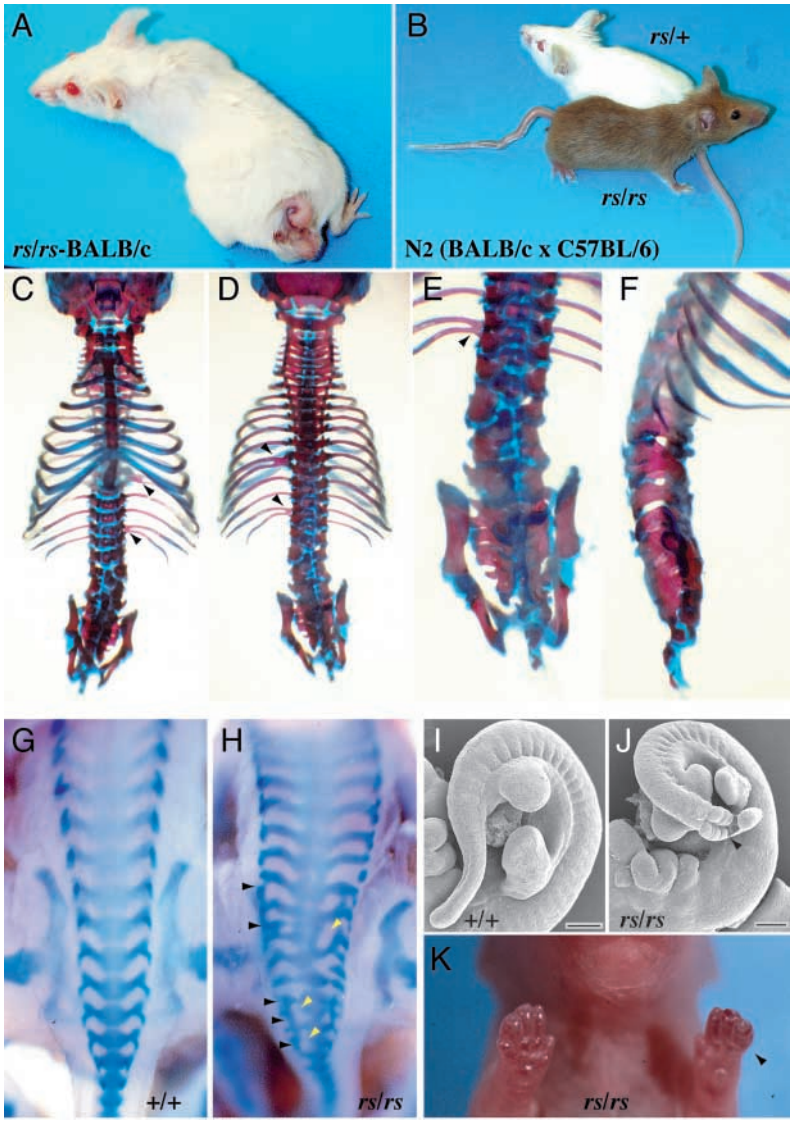

Fig. 1. Dysmorphologies in *rs* mutants. (A) A typical *rs/rs* animal with the original BALB/c background and (B) *rs/rs* and *rs/+* animals with BALB/c-C57BL/6 mixed backgrounds. (C-F) Vertebrae from newborn *rs/rs* viewed from the ventral (C), dorsal (D,E), or right-lateral (F) sides. (G,H) Alcian Blue-stained E14 skeletons (dorsal view) from control (G) and *rs/rs* (H) show vertebral segmentation defects. Note neural arch fusion (black arrowheads in H) and its loss (yellow arrowheads in H). (I,J) SEM of control (I) and *rs/rs* (J) embryos at E11 shows neural tube closure defects in the lumbo-sacral region (the arrowhead in J). (K) Oligodactyly (arrowhead) is occasionally observed in *rs/rs*. Scale bars: 100 μm.

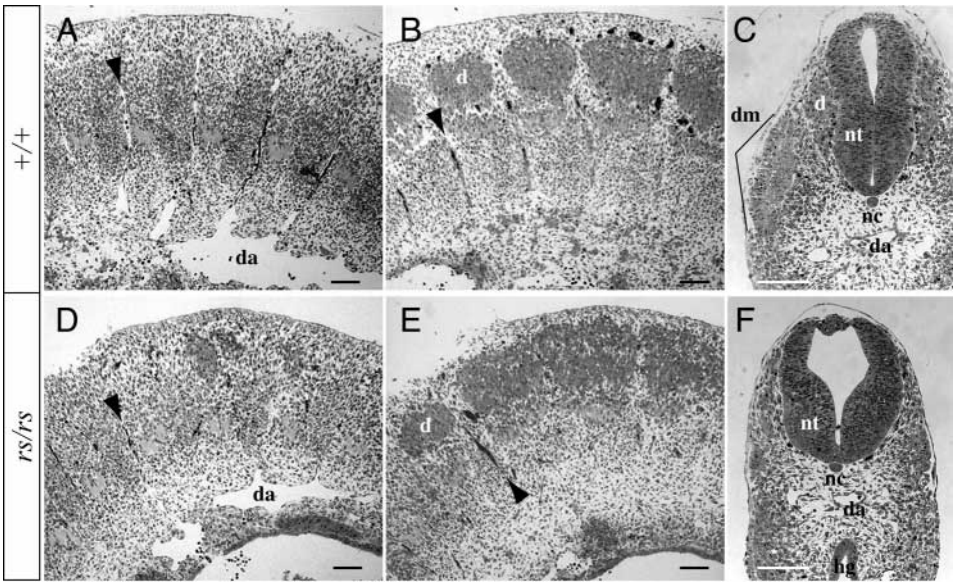

Fig. 2. Histology of the lumbar region of *rs* embryos at E11. (A,B,D,E) On the sections (A,D, near midsagittal; B,E, parasagittal; the rostral side is to the left of each panel), somite borders demarcated by intersegmental vessels (arrowheads in A,B,D,E) are clearly visible in the control (A,B), whereas they are unclear in *rs/rs* (D,E). DRGs (d in B,E) are fused in *rs/rs* (E), while they are clearly segmented in controls (B). (C,F) Transverse sections at a proximal tail region from control (C) and *rs/rs* (F) embryos reveal malformations of the neural tube in *rs/rs*. The epithelial organization of dermomyotome (dm in C) is disturbed in *rs/rs* (F). da, dorsal aorta; hg, hindgut; nc, notochord; nt, neural tube. Scale bars: 100 μm.

epithelialization of somites, and the somite AP polarity were disturbed in *rs* mutants.

ringelschwanz is a hypomorphic allele of *Lrp6*

A total of 461 progeny from the backcross mating between N_1 (C57BL/6 × *rs/rs*-BALB/c) females and *rs/rs*-BALB/c males was used for genetic mapping. The *rs* locus was located on chromosome (Chr) 6 at about 64 cM from the centromere in the interval between *D6Mit374* and *D6Mit339*, with the following locus order: centromere – *D6Mit374* – 0.87±0.43 cM – *rs* – 0.43±0.31 cM – *D6Mit339* – telomere (see Fig. S1 in the supplementary material). *D6Mit301* was non-recombinant with *rs* in this backcross panel. During the course of backcross mapping, we noticed strong genetic background effects on the *rs* phenotype, as a majority of *rs/rs* N_2 mice exhibited significantly milder tail malformations (Fig. 1B). Based on our own radiation hybrid mapping data (data not shown), the mouse *rs* critical interval corresponded to a human genome segment flanked by *ETV6* and *LMO3* on human Chr 12p12. We found 17 named genes in this interval, and by RT-PCR and sequencing of mouse counterparts of these genes in *rs* mutants, we found a missense mutation in *Lrp6* by a transition of C at nucleotide 2741 (according to GenBank NM_008514) to T, leading to an amino acid substitution of Trp for Arg at codon 886 (Fig. 3A). We established a PCR-based genotyping method detecting this mutation in *rs* as the absence of the *Hpa*II site (CCGG in wild-type is CTGG in *rs*). This nucleotide substitution was specific in *rs*, and was not present in BALB/c and C57BL/6 (Fig. 3B). In the backcross panel, *Lrp6*, genotyped by this method, was not recombinant with *rs* (see Fig. S1 in the supplementary material). The Arg residue at codon 886 of Lrp6 was located in the dickkopf-binding region (Zorn, 2001; Mao et al., 2001a), notably between the third YWTD β-propeller domain (Jeon et al., 2001; Takagi et al., 2003) and the third EGF-like repeat (Fig. 3C). This Arg residue was highly conserved among Lrp family proteins in diverse species (Fig. 3D). Furthermore, previously reported *Lrp6*-null mutant phenotypes in the mouse resemble those in *rs* mutants, although the null phenotypes were much more severe (Pinson et al., 2000). Thus, a line of evidence strongly suggested that *rs* was an allele of *Lrp6*. We tested this possibility by a genetic complementation test using the *Lrp6*-null mutant mice. Approximately one-quarter of offspring from mating pairs between $Lrp6^{+/-}$ and *rs/+* heterozygotes exhibited expected phenotypes with intermediate severities between those of $Lrp6^{-/-}$ and *rs/rs* (Fig. 4A). Morphological and skeletal analyses of E14.5 fetuses of compound mutants ($rs/Lrp6^{-}$) in comparison to those of $Lrp6^{-/-}$, *rs/rs* and wild-type demonstrated a gradient in the severity of the dysmorphology phenotypes as shown in Fig. 4B-I. $Lrp6^{-/-}$ mutants showed a variety of externally visible, severe malformations as exemplified in Fig. 4E. $rs/Lrp6^{-}$ mutants exhibited significantly less severe defects, but were definitely more significantly affected than *rs/rs* mutants. The level at which axial truncation usually occurred was clearly different in each of the three genotypes: $Lrp6^{-/-}$ at the lumber region, $rs/Lrp6^{-}$ at the sacral region and *rs/rs* in the proximal tail region (Fig. 4F-I). Thus, we genetically confirmed that *rs* was a hypomorphic allele of *Lrp6*. The name of the mutation '*ringelschwanz*' and its symbol '*rs*' have been registered to the MGI database as an allele of *Lrp6* with the reference no. MGI:2673982.

Canonical Wnt/β-catenin pathway is defective in *rs*-derived fibroblasts

In order to assess whether the canonical Wnt pathway was defective in *rs* mutants, we performed an in vitro assay with primary fibroblasts obtained from *rs* mutants (Fig. 5). When the two effectors of the canonical Wnt pathway, Lef1 and β-catenin, were overexpressed by transfection into fibroblasts, activation of the luciferase reporter was observed in *rs/rs* cells (rs3 and rs8), as well as in control cells (rs5 and rs7) from wild-type and *rs/+* animals, respectively. However, when Wnt1 was overexpressed instead of β-catenin, the reporter activity was dramatically reduced in *rs/rs* cells. There was a slight reduction in the reporter activity also in the case of *rs/+* cells, suggesting the semi-dominant nature of Lrp6 insufficiency as assessed by this assay. This result indicated that the mutated protein $Lrp6^{rs}$

could not efficiently mediate the Wnt/β-catenin signal transduction pathway.

Somite anteroposterior (AP) polarity defects in *ringelschwanz* mutants

Our dysmorphology examinations on *rs* mutants demonstrated disturbances in somite formation in the lumbo-sacral-tail region. In order to clarify these disturbances in *rs* at the molecular level, we performed a marker expression study. We first examined the expression pattern of *Sox10* as a marker for cells in DRGs of neural crest origin (Fig. 6A,B). The segmental organization of the DRGs was disturbed at the hindlimb level. We then tested expression patterns of somite marker genes that were differentially expressed in either the anterior or the posterior somite compartment. A T-box transcription factor, *Tbx18*, was predominantly expressed in the anterior halves (Fig. 6C) (Kraus et al., 2001), while a paired-type homeobox gene, *Uncx4.1*, was exclusively expressed in the posterior halves (Fig. 6E) (Leitges et al., 2000; Mansouri et al., 1997). Expression of *Tbx18* in *rs* embryos was highly abnormal, such that the *Tbx18*-positive domain extended to the posterior half of somites in the lumbar region and the *Tbx18*-positive domains progressively became continuous in a rostro-caudal direction (Fig. 6D). However, expression of *Uncx4.1* in *rs* embryos appeared fairly normal until the lower thoracic region, and then it became progressively fainter and more diffuse in the caudal part (Fig. 6F). Taken together, these results suggested that the somite AP polarity was affected in *rs*, with no discrete somite AP compartments being established from the lumbar region onwards.

Somite epithelialization defect in *rs* is not due to paraxis-deficiency

The bHLH transcription factor paraxis (Tcf15 – Mouse Genome Informatics) is required for the formation of epithelial somites and the maintenance of the somite AP polarity (Burgess et al., 1996; Johnson et al., 2001). Therefore, the observed defects in somite polarity and epithelialization in *rs* embryos could be attributed to paraxis deficiency. Interestingly, expression of paraxis was well maintained in *rs* (Fig. 6H,J). The initiation and strong upregulation of paraxis in the rostral part of the PSM were clearly confirmed in *rs*, despite the severe morphological disturbances in the caudal part of mutant embryos (Fig. 6I,J). Thus, we concluded that paraxis is not responsible for the polarity and epithelialization defects in *rs* somites. Since paraxis can be regarded as a paraxial/somitic mesoderm-specific marker, the presence of paraxis-positive cells in *rs* also indicates that paraxial mesoderm cells are still present or specified in the highly malformed tail of *rs/rs* embryos.

Dysfunction of the somite segmentation clock in *rs*

The notch-delta signaling pathway is known to play an essential role in somitogenesis as part of the segmentation clock machinery that drives periodic formation of somites (Pourquié, 2001). Thus, we examined expression of some key players in the notch-delta pathway, including *Dll1*, *Mesp2* and *Lfng*, in *rs* embryos. *Dll1* was normally expressed very strongly in the PSM, except in prospective anterior-half compartments in the rostral part of the PSM (Bettenhausen et al., 1995). In *rs* mutants, expression of *Dll1* appeared indistinguishable from that in wild-type controls until early E9 (Fig. 7A,B). Remarkably, while strong expression of *Dll1* in the caudal two-thirds of the PSM was well maintained, expression of *Dll1* in a striped pattern in the rostral PSM was disturbed in *rs* embryos at mid to late E9 (Fig. 7C-F). At early E10, *Dll1* expression in the caudal PSM of *rs* mutants was significantly reduced (Fig. 7H, compared with G), and by mid E10, *Dll1* expression in the PSM was totally abolished (Fig. 7I). Cyclic expression of *Lfng* in the PSM reflects the activity of the segmentation clock (Evrard et al.,

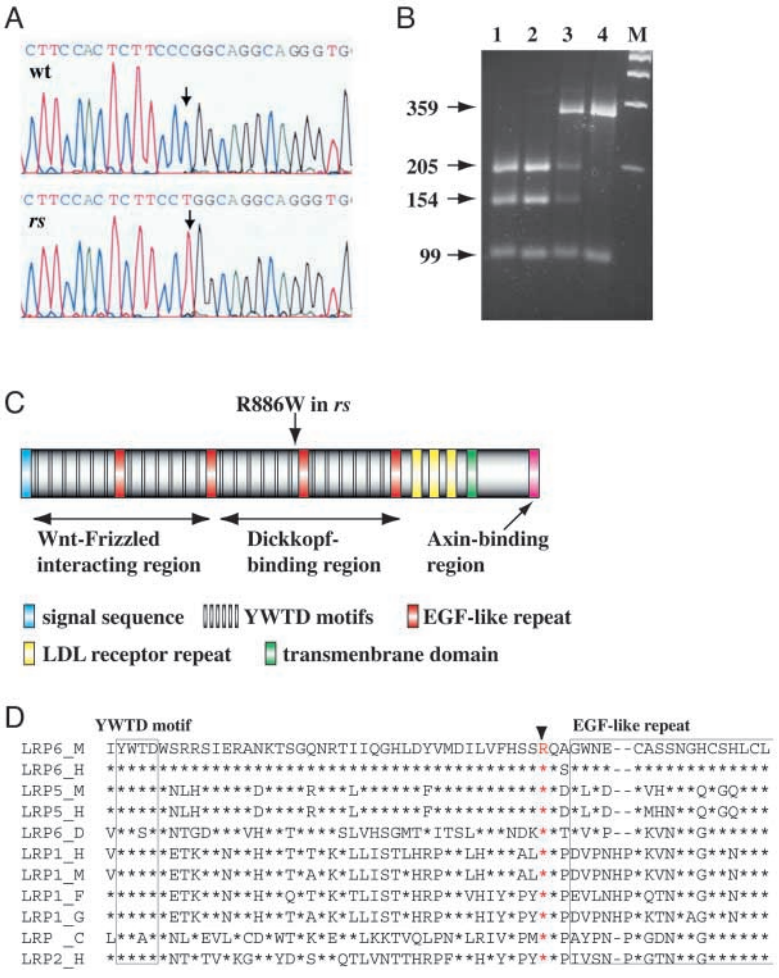

Fig. 3. Mutation detection in *Lrp6*. (A) Chromatograms show the C to T transition in *rs*. (B) PCR-based genotyping with *Hpa*II digestion. In wild-type (BALB/c and C57BL/6 in lanes 1 and 2, respectively), the 458-base product from wild-type is cut into three fragments (205, 154 and 99 bases), while one from *rs* into only two fragments (359 and 99 bases) (Lane 4). Heterozygous specimens show four fragments (359, 205, 154 and 99 bases) (lane 3). (C) A schematic drawing of the Lrp6 protein structure with designations for known functional domains. The *rs* mutation resides right in front of the third EGF-like repeat. (D) The Arg (R) residue at the corresponding positions is highly conserved among various Lrp proteins. Designations after Lrp: M, mouse; H, human; D, *Drosophila*; F, *Xenopus*; C, *C. elegans*.

1998). Consistent with the progressive downregulation of *Dll1* in the PSM of *rs* embryos, *Lfng* expression in the PSM was also strongly downregulated by mid E10 (Fig. 7O, compared with N). Interestingly, *Mesp2* expression in the rostral part of the PSM appears to be maintained for a longer time, although at a reduced level, even at mid to late E10 in *rs* embryos (n=20) (Fig. 7J-M).

Recently a proliferative role of Wnt3a in the chick PSM was reported (Galli et al., 2004). Cell proliferation defects may explain the cellular basis of these somitogenesis defects in *rs* mutants. Thus we examined the status of cell proliferation and programmed cell death by BrdU incorporation and TUNEL assays, respectively. To our surprise, we could not observe any significant differences in these aspects of cellular statuses (Fig. 8).

Delayed ossification in *rs* mice

As shown in Fig. 9, skeletal preparations at the P0 stage

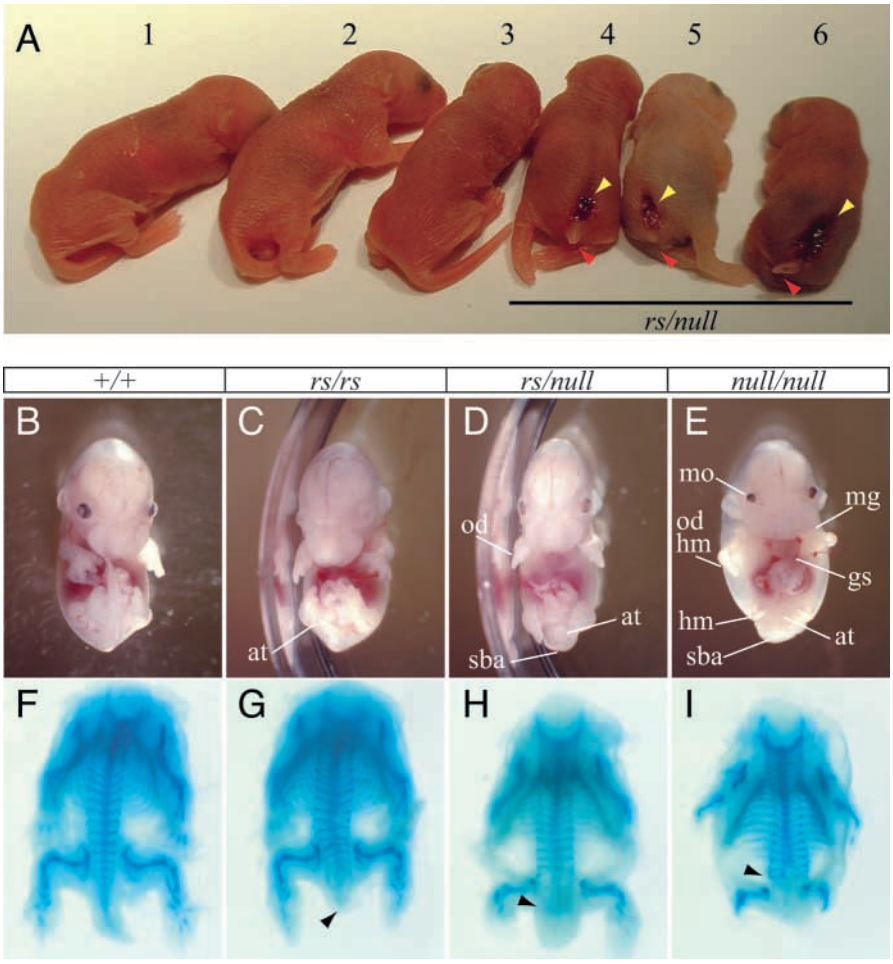

Fig. 4. Non-complementation between the *rs* mutation and a null allele of *Lrp6*. The *Lrp6*-null allele is designated as *null*. (A) Compound heterozygotes (*rs/null*), obtained from mating between *rs*/+ and *null*/+ at the newborn stage, exhibit a rudimentary tail (red arrowheads) and spina bifida aperta (yellow arrowheads) (4-6). (1-3) are either of +/+, *rs*/+, or *null*/+. (B-I) E14 fetuses of *rs/rs* (C,G), *rs/null* (D,H), or *null/null* (E,I) genotypes exhibit a clear gradient in the severity of the dysmorphology phenotypes, both externally (B-E) and internally (F-I). Note the presence of a variety of morphological defects in *null/null* (E), including micropthalmia (mo), micrognathia (mg), oligodactyly (od), hypomelia (hm), gastroschisis (gs), spina bifida aperta (sba) and axial truncation (at). In the skeletal samples (F-I), note the difference in the levels of axial truncation (arrowheads).

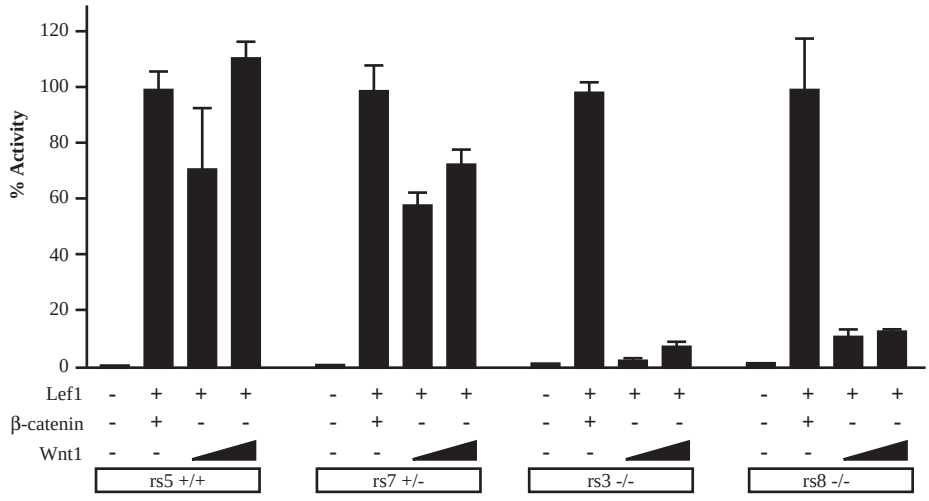

Fig. 5. Transcriptional activation by LEF1 in response to Wnt1 signaling in primary-cultured fibroblasts from newborns. Fibroblasts of rs5 (+/+), rs7 (*rs*/+), rs3 (*rs/rs*) and rs8 (*rs/rs*) were transfected with a LEF-LUC reporter construct (500 ng), in combination with expression plasmids encoding LEF1 (50 ng), β-catenin (300 ng) or Wnt1 (300 or 1000 ng). The levels of luciferase activity were normalized for the expression of a co-transfected Rous sarcoma virus-β-galactosidase expression plasmid (50 ng). The normalized activity was quantitated relative to the level of activity (100%) from cells transfected with LEF1 and β-catenin expression plasmids. Means with error bars representing standard errors. Experiments were repeated at least three times.

revealed that the appearance of ossification centers in the metatarsal and phalangeal bones in 50% (n=10) of P0 specimens was delayed compared with wild-type littermates (Fig. 9A,B). Histology of hindlimbs from the contralateral side of the same P0 specimens showed that in the cartilaginous anlage of a phalangeal bone undergoing the process of endochondral ossification, the zones of resting, proliferating, prehypertrophic and hypertrophic chondrocytes could be distinguished in *rs/rs*, however, the layer of prehypertrophic chondrocytes (ph in Fig. 9E,F) appeared slightly reduced in *rs/rs* compared with the control.

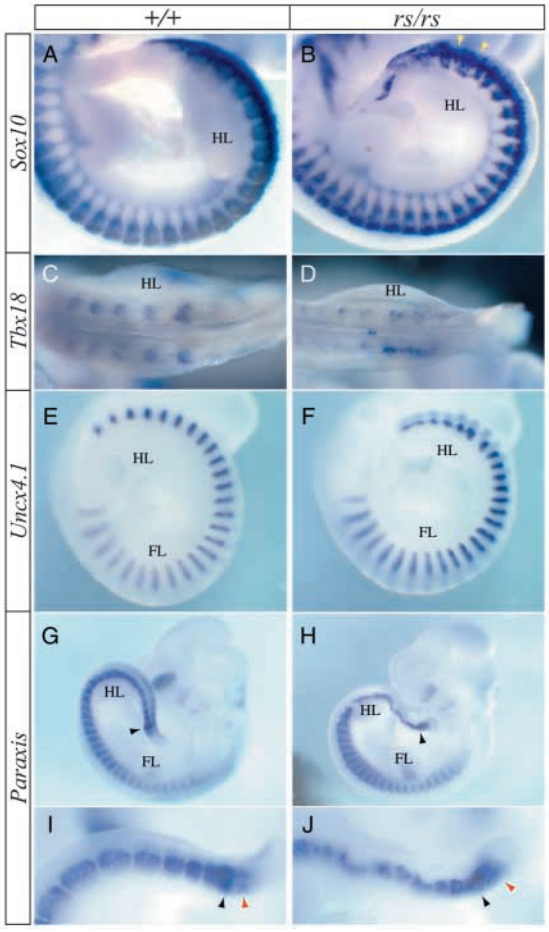

Fig. 6. Disturbance in the AP polarity of somites and preserved expression of paraxis in *rs* mutants. Whole-mount in situ hybridization of *rs/rs* embryos (B,D,F,H,J) compared with stage-matched control embryos (A,C,E,G,I) at early E10 (A-F) and late E10 (G-J) with probes for *Sox10* (A,B) *Tbx18* (C,D), *Uncx4.1* (E,F) and paraxis (G-J). (A-F) *Sox10*-positive domains show the status of segmentation of the DRGs. In *rs/rs*, DRG segmentation in the caudal region is disturbed (yellow arrowheads in B). Expression patterns of *Tbx18* and *Uncx4.1* in *rs/rs* in somites rostral to the hindlimb bud are fairly normal and are restricted to the anterior and posterior compartments, respectively. In more caudal regions, their expression patterns become diffuse in *rs/rs*. (G-J) Expression of paraxis is well maintained in *rs/rs* (overviews in G,H; magnified views in I,J). Both the initiation of paraxis expression in the PSM (red arrowheads in I,J) and its strong upregulation in the rostral PSM (black arrowheads in G-J) take place normally in *rs/rs*. FL, forelimb buds; HL, hindlimb buds.

Osteoporosis in adult *rs* mice

We next examined the integrity of adult bones in *rs* mutants. The status of lumbo-sacral vertebrae in 9-month-old *rs/rs* and its control animal was examined by X-ray radiography (Fig. 10A,B). Aside from the strong vertebral malformations in *rs/rs*, vertebrae were more translucent in *rs*. Consistently, on histological sections the reductions in the number of trabecules and in the thickness of the cortical bone were remarkable in *rs* (Fig. 10C,D). Interestingly, a clump of cells of chondrocytic morphology (arrowhead in Fig. 10F) was frequently seen in *rs*, suggesting the presence of foci undergoing the recovery process from multiple microfractures. In order to quantitatively assess bone density and cortical bone thickness, we further performed a peripheral quantitative computed tomography (pQCT) analysis on the proximal part of the tibia from 14 month-old female animals, and the summary of pQCT data from the metaphysis region of the tibia is shown in graphs (Fig. 10G-I). In *rs/rs*, the bone density was significantly reduced to 84% of wild-type controls in the whole metaphysis (P<0.05) (Fig. 10G) and to 94% in cortical bones (P<0.01) (Fig. 10H). In the metaphysis, the cortical bone thickness was significantly reduced to 71% of wild-type controls (P<0.01) (Fig. 10I). *rs/+* samples exhibited intermediate values between wild-type and *rs/rs*, suggesting the semidominant nature of the *rs* mutation with respect to these traits. Thus, we demonstrated the presence of a low bone mass phenotype in *rs* mutants, which was similar to that of Lrp5 mutants.

Discussion

In the present study, we have demonstrated, for the first time, that Lrp6 is required for normal somitogenesis in the PSM and for the control of osteogenesis and bone volume. Although not addressed here, *rs* mutant mice can certainly serve as a mouse model for neural tube defects and limb dysmorphologies including oligodactyly in humans caused by WNT signaling defects.

Wnt/Lrp6 pathway in somitogenesis

The morphogenetic movement to form somites is regarded as the intrinsic property of the PSM. However, some extrinsic signal(s) from the overlaying surface ectoderm is required to complete somite segmentation (Borycki et al., 2000; Correia and Conlon, 2000; Sosic et al., 1997). The bHLH transcription factor paraxis is thought to mediate this extrinsic signal (Correia and Conlon, 2000; Sosic et al., 1997), and paraxis deficiency leads to disturbances in the epithelialization and AP polarity determination of somites (Burgess et al., 1996; Johnson et al., 2001). Thus we assumed that defects in somitogenesis in *rs* might be in part due to paraxis deficiency. However, we found that paraxis expression is unexpectedly well maintained in *rs* mutants, suggesting the presence of additional player(s) that is/are controlled by Wnt signaling.

Notch-delta signaling is required for the upregulation of *Mesp2* in the rostral PSM, and the induced Mesp2 in turn represses *Dll1* (Takahashi et al., 2000). In the prospective somite posterior halves at the somite stage I level (Pourquié and Tam, 2001), where *Mesp2* expression has been downregulated, *Dll1* is re-upregulated via Psen1-dependent notch-delta signaling (the notch-delta-Mesp2 regulatory loop) (Takahashi et al., 2000; Saga and Takeda, 2001). Thus, our

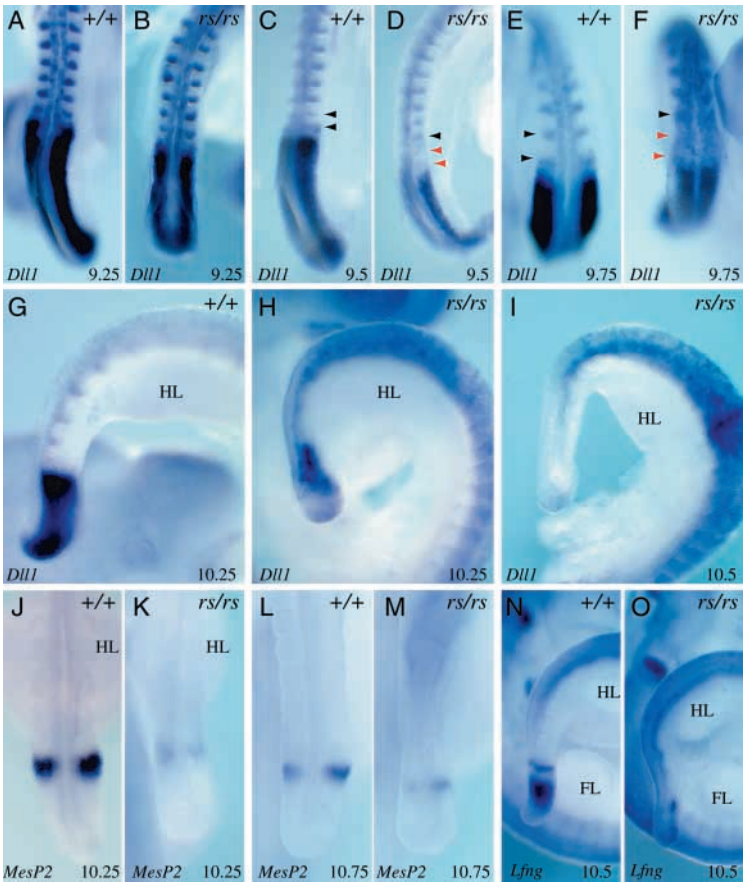

Fig. 7. Disturbances in expression of notch-delta pathway genes in *rs* mutants. Whole-mount in situ hybridization of *rs/rs* embryos (B,D,F,H,I,K,M,O) compared with stage-matched control embryos (A,C,E,G,J,L,N) at carefully selected stages of E9 (A-F) and of E10 (G-O) with probes for *Dll1* (A-I), *Mesp2* (J-M) and *Lfng* (N and O). Expression of *Dll1* in *rs/rs* appears fairly normal up to E9.5 (B). However, stripe-like expression of *Dll1* in the rostral PSM and in newly formed somites (black arrowheads in C-F) becomes unclear and less intense (red arrowheads in D,F) from E9.5 on (D), while strong *Dll1* expression in the caudal two-thirds of the PSM is still maintained during late E9 (F), starts to reduce from early E10 (H), and diminishes by mid E10 (I). Surprisingly, *Mesp2* expression in a stripe pattern in the rostral PSM continues, though significantly reduced in intensity, until late E10 in *rs/rs* (K,M). Dynamic and oscillating expression of *Lfng* in the PSM is also observed until early E10, but appears to cease by mid E10 in *rs/rs* (O). FL, forelimb buds; HL, hindlimb buds.

observation that this *Dll1* re-upregulation is disturbed in *rs* mutants suggests that this process of *Dll1* re-upregulation is also dependent on Wnt signaling. This finding points to the possibility of the regulatory interactions between the Wnt and notch-delta signaling pathways in the control of somitogenesis at the rostral part of the PSM. The present study does not define when and how Wnt signaling is required for the maintenance of the notch-delta-Mesp2 regulatory loop. Further study is needed to address these issues.

In the PSM of *rs/rs*, we could not detect significant change in the status of cell proliferation and programmed cell death (Fig. 8). This suggests that the apparent reduction in the number of cells in the PSM corresponding to the sacral and tail region of *rs/rs* mutants is mainly due to the reduction in the rate of production of paraxial mesoderm cells in the tail bud. Recently, Wnt3a signaling has been implicated in the proliferation of PSM cells in the chick (Galli et al., 2004), but our observation appears inconsistent with this notion. The proliferative role of Wnt3a in the chick is proposed based on observations from overexpression studies. Thus, our result from a loss-of-function study in *rs* may not necessarily be contradictory. With noting the hypomorphic nature of the *rs* mutation, we do not rule out the possibility that Lrp6-mediated Wnt signaling is indeed required for cell proliferation in the PSM.

Genetic factors for the pathogenesis of vertebral segmentation defects

In humans, a number of hereditary disorders with vertebral segmentation defects have been reported. However, the molecular pathogenesis remains unknown in most cases. Spondylocostal dysostosis is one form of vertebral segmentation defect, and involves characteristic rib malformations with proximal fusions, called crab-like chest. Vertebral segmentation defects in *rs* mice, due to the disturbances in somitogenesis, are frequently associated by rib fusions at the proximal part (Fig. 1C-E). Thus, Lrp6 may be one of genetic factors for the pathogenesis of spondylocostal dysostosis in humans.

In the mouse, a group of classical mutations, collectively referred to as ‘Wirbel-Rippen-Syndrom (vertebra-rib syndrome)’ (Theiler, 1968; Theiler, 1988), including *Crooked tail* (Morgan, 1954), *Malformed vertebrae* (Theiler et al., 1975), *pudgy* (Grüneberg, 1961), *Rachiterata* (Theiler et al., 1974), *Rib fusions* (Theiler and Stevens, 1960), *Rib-vertebrae* (Theiler and Varnum, 1985) and *Fused* (Theiler and Glücksohn-Wälsch, 1956), affect vertebral segmentation with rib malformations. Their characteristic dysmorphologies in the vertebrae and ribs strikingly resemble those seen in individuals suffering from spondylocostal dysostosis. Indeed, *delta-like 3* (*Dll3*), encoding a ligand for the notch receptor, has been shown to be mutated in the *pudgy* mutation in the mouse (Kusumi et al., 1998). Accordingly, the human counterpart *DLL3* is mutated in the Jarcho-Levin syndrome, an autosomal recessive hereditary disorder, representative of spondylocostal dysostosis in humans (Bulman et al., 2000). On the other hand, *Axin*, encoding a negative regulator of the Wnt/β-catenin signaling pathway, was identified as a gene disrupted in an allelic series of *Fused* (Zeng et al., 1997). Furthermore, vertebral column malformations of knockout mutants in lunatic fringe (Lfng) (Evrard et al., 1998; Zhang and Gridley, 1998) and *Hes7* (Bessho et al., 2001) also phenocopy spondylocostal dysostosis symptoms, thus they can also be regarded as mouse models for spondylocostal dysostosis. It should be noted that these genes discussed here are components of the notch-delta or Wnt pathways in somitogenesis. This notion is consistent with the emerging view from the recent studies (Aulehla et al., 2003; Hamblet et al., 2002) and our present work that somitogenesis is controlled by a concerted interaction between the notch-delta and Wnt signaling pathways. It is thus conceivable that various components of the notch-delta and Wnt pathways comprise

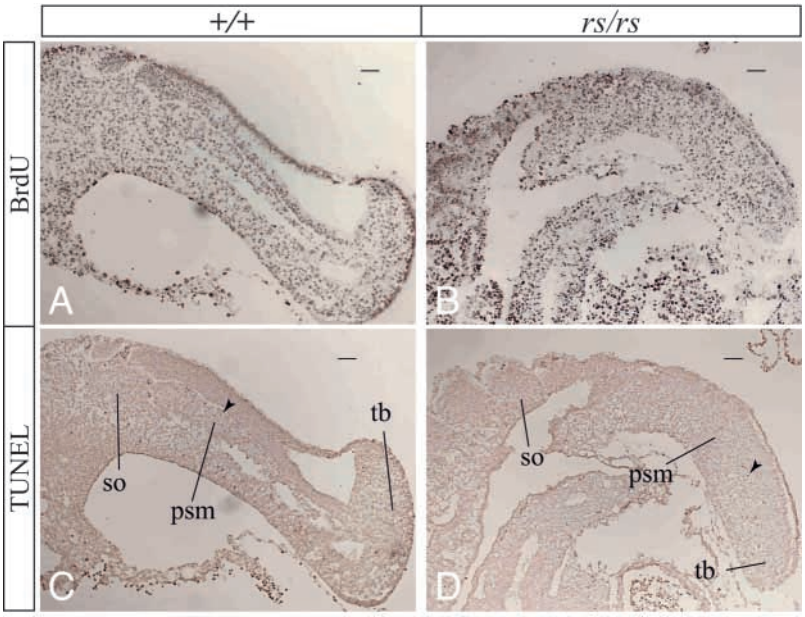

Fig. 8. Cell proliferation and programmed cell death in the PSM of *rs/rs*. BrdU incorporation (A,B) and TUNEL (C,D) assays were performed on serial frozen sections of E10.5 control (A,C) and *rs/rs* (B,D) embryos. Note that a number of BrdU-positive cells are present in the PSM (psm) as well as in somites (so) of both *rs/rs* (B) and control (A). The numbers of apoptotic cells detected by TUNEL in the PSM (examples indicated by the black arrowheads in C,D) are comparable between control and *rs/rs*. Tb, tail bud. Scale bars: 100 μm.

genetic factors for the pathogenesis of vertebral segmentation defects including spondylocostal dysostosis. As discussed below, in *rs* mutants, delayed ossification and osteoporosis associate with vertebral segmentation defects. Since the notch-delta pathway has not been implicated in osteogenesis, this association might be of diagnostic importance in sorting out the potential molecular etiology of individuals with vertebral segmentation defects.

Lrp6 as a novel genetic factor for osteoporosis

Our analyses of *rs* animals at postnatal stages revealed two types of bone defects. First, a delay in ossification in *rs* mutants was confirmed in phalangeal bones in fingers and toes, which is very similar to that reported for Lrp5-null mice (Kato et al., 2002). Our histological analysis suggests that this defect is probably secondary to preceding disturbances in chondrocyte differentiation in the context of endochondral ossification. Indeed, our preliminary analysis of embryos between E14 and E18 suggests that delayed ossification is a general problem in *rs* mutants, because it is also present in other bones including the zeugopod and stylopod of the limbs (data not shown). Second, bone density and mass are reduced, which are also similar to those in *Lrp5*-deficient mice. Lrp5 and Lrp6 are highly similar in the primary structure and in the function as coreceptors in Wnt signaling. Furthermore, both *Lrp5* and *Lrp6* are induced by bmp2 treatment in osteoblastic ST2 cells (Gong et al., 2001). Thus, it is very likely that there is a functional redundancy between Lrp5 and Lrp6 in bone formation. Indeed, a genetic interaction between Lrp5 and Lrp6 has recently been demonstrated during osteogenesis and during gestation (Kelly et al., 2004). We confirmed co-expression of Lrp5 and Lrp6 in embryonic fibroblasts by RT-PCR (see Fig. S2 in the supplementary material). Nevertheless, our in vitro assay system to assess the function of the mutated Lrp6 could detect significantly reduced Wnt signal transduction in *rs/rs* (Fig. 5).

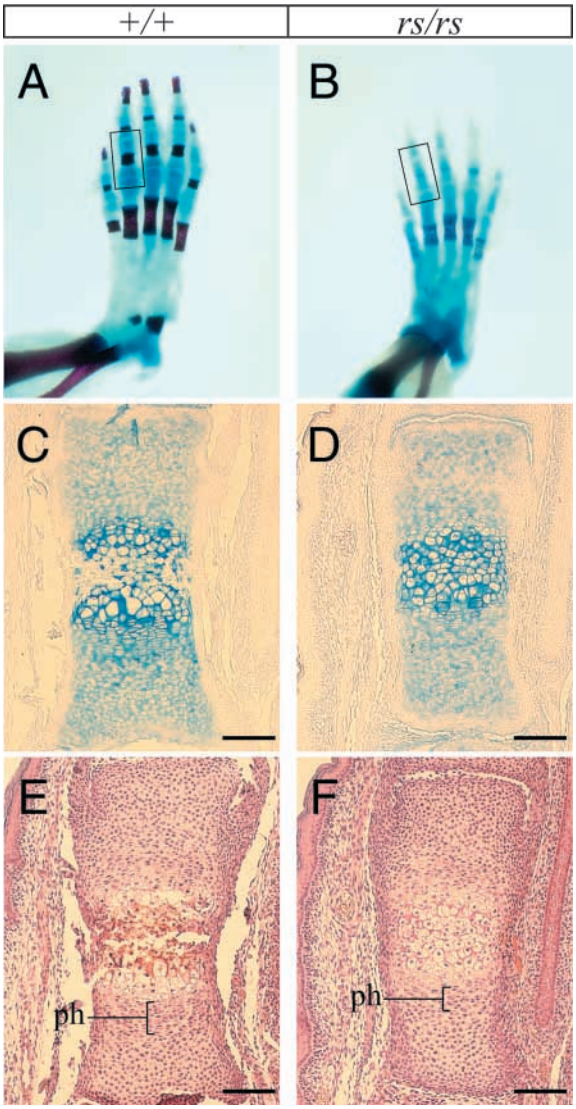

Fig. 9. Delayed ossification in *rs/rs*. (A,B) Skeletal analysis at the newborn stage revealed delayed ossification in metatarsal and phalangeal bones of the hindlimb (dorsal view, right side) from wild-type (A) and *rs/rs* (B). (C-F) Histology of non-decalcified bones from the contralateral (left) side of the hindlimbs from the same newborn animals. The corresponding areas is indicated by the boxes in A and B (the proximal phalanx of the second toe). In C and D, sections are stained by Alcian Blue, while sections are stained Alizarin Red and hematoxilin in E,F. Note the absence of Alizarin Red staining in the region of chondrocyte hypertrophy. The zone of prehypertrophic chondrocytes starting to undergo hypertrophy (brackets with ph in E,F) seems reduced in *rs/rs*. Scale bars: 100 μm.

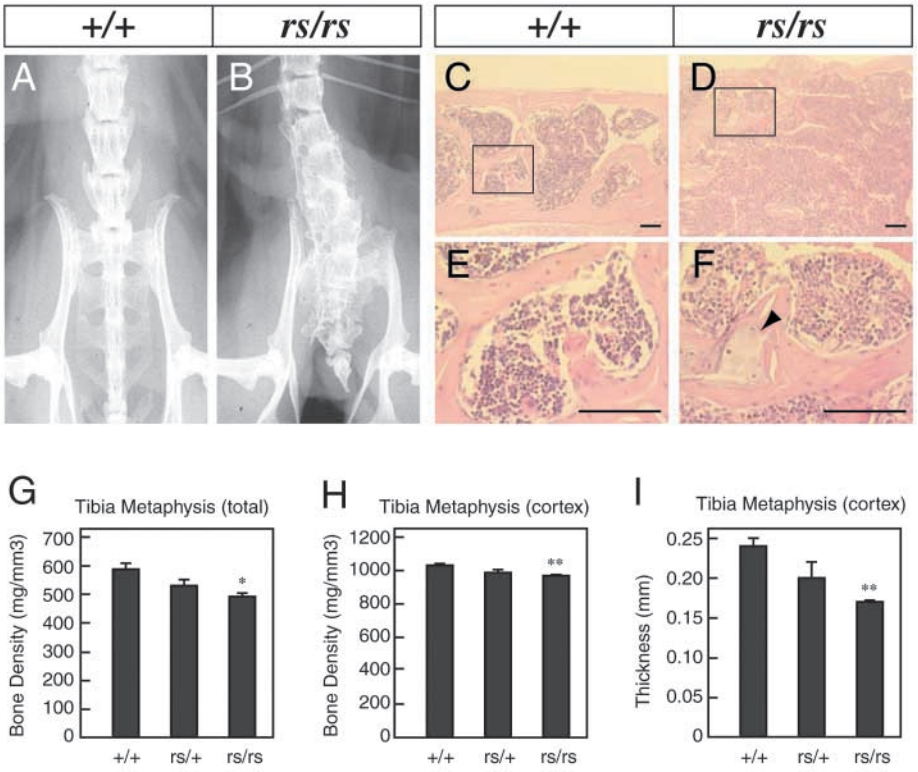

Fig. 10. Osteoporosis in *rs/rs* adult mice. (A-F) X-ray radiography (A,B) and histology (C-F) of the lumbo-sacral vertebrae were carried out in *rs/rs* (B,D,F) and control (A,C,E) animals. The boxed areas in C and D are shown at a higher magnification in E and F, respectively. The arrowhead in F points to a group of chondrocytes inside the trabecule. Scale bars: 50 μm. (G-I) Low bone mass phenotype in *rs* mutants demonstrated by pQCT. Bone density and the thickness of cortical bones in the metaphysis of the tibia were measured in *rs/rs*, *rs/+* and +/+ animals (14 month-old females in triplicate for each genotype), and results are graphically depicted for bone density measures from total tibial metaphysis (G) and the cortex part (H), and for the cortical bone thickness (I). Values represent the means + standard errors. Single and double asterisks indicate statistically significant reductions ($P<0.05$ and $P<0.01$, respectively) in *rs/rs* compared with +/+.

These observations together suggest that the contribution made by either Lrp5 or Lrp6 in their cooperation may significantly vary, presumably in a tissue-specific manner. This idea is consistent with the notion that Lrp6 functions more significantly than Lrp5 at least during gestation (Kelly et al., 2004).

The strong malformations in the axial skeleton in *rs* mutants are, surprisingly, not associated with disturbances in nerve functions that affect locomotion. Therefore, at least, the observed osteoporosis phenotype in *rs* mutants is unlikely to be a secondary consequence of the vertebral malformations. Whether Lrp6, like Lrp5, positively regulates osteoblast proliferation and function is currently under investigation. Further study is required to define how the functional roles of Lrp5 and Lrp6 are shared in the control of bone development and homeostasis. If Lrp5 and Lrp6 function redundantly also in adult bones, pharmacological activation of Lrp6-mediated signaling can be a therapeutic means even in LRP5-deficient individuals suffering from osteoporosis.

Our observation that *rs/+* animals show a slight decrease in bone mass suggests that the function of Lrp6 in bones is haploinsufficient. A similar dosage effect has been observed for Lrp5 in humans and mice: *Lrp5*-null heterozygotes exhibit reduced bone mass (Gong et al., 2001; Kato et al., 2002). Together with the notion that activating mutations in Lrp5 increases bone mass in a dominant manner (Boyden et al., 2002; Little et al., 2002), these observations suggest that the activity of the Wnt canonical pathway may have to be tightly regulated within a certain range with the intact two copies of each of the *Lrp5* and *Lrp6* genes.

Recent studies on Lrp5 have also shed light on its unexpected roles in cholesterol metabolism and in glucose-induced insulin secretion, thereby its potential involvement in atherosclerosis and in diabetes has been indicated (Magoori et al., 2003; Fujino et al., 2003). It is currently not known whether Lrp6 exerts similar functions in these biological processes. However, these issues can certainly be addressed in the *rs* mutant mouse line by taking advantage of the hypomorphic nature of the *Lrp6* mutation. Thus, it is conceivable that future studies with *rs* mutant mice will bring further so-far uncovered insights into Lrp6 functions in both the pre- and postnatal stages.

We thank Rudi Balling, Chisa Shukunami, Laure Bally-Cuif and her laboratory members for helpful discussions and comments on this work; Jack Favor for critical reading of the manuscript; William C. Skarnes for *Lrp6*-null mice; Johann Kummermehr and Iris Baur for their skillfull technical support in preparing the acrylate sections; Kenta Yashiro, Hidetoshi Taniguchi and Masako Taniike for valuable technical advice; Helga Wehnes and Luise Jennen for technical helps in histology; Kornelia Fieder for animal work; Hiroshi Hamada and Junji Takeda for providing a generous research environment. This work was supported in part by a grant from the GSF-National Research Center for Environment and Health (to K.I.), and in part by a grant from Japanese Ministry of Education, Culture, Sports, Science and Technology (to K.O.).

Supplementary material

Supplementary material for this article is available at
http://dev.biologists.org/cgi/content/full/131/21/5469/DC1

References

Aulehla, A., Wehrle, C., Brand-Saberi, B., Kemler, R., Gossler, A., Kanzler, B. and Herrmann, B. G. (2003). Wnt3a plays a major role in the segmentation clock controlling somitogenesis. *Dev. Cell* **4**, 395-406.

Bafico, A., Liu, G., Yaniv, A., Gazit, A. and Aaronson, S. A. (2001). Novel mechanism of Wnt signalling inhibition mediated by Dickkopf-1 interaction with LRP6/Arrow. *Nat. Cell Biol.* **3**, 683-686.

Bessho, Y., Sakata, R., Komatsu, S., Shiota, K., Yamada, S. and Kageyama, R. (2001). Dynamic expression and essential functions of Hes7 in somite segmentation. *Genes Dev.* **15**, 2642-2647.

Bettenhausen, B., Hrabe de Angelis, M., Simon, D., Guenet, J. L. and Gossler, A. (1995). Transient and restricted expression during mouse embryogenesis of Dll1, a murine gene closely related to Drosophila Delta. *Development* **121**, 2407-2418.

Borycki, A., Brown, A. M. and Emerson, C. P., Jr (2000). Shh and Wnt signaling pathways converge to control Gli gene activation in avian somites. *Development* **127**, 2075-2087.

Boyden, L. M., Mao, J., Belsky, J., Mitzner, L., Farhi, A., Mitnick, M. A., Wu, D., Insogna, K. and Lifton, R. P. (2002). High bone density due to a mutation in LDL-receptor-related protein 5. *N. Engl. J. Med.* **346**, 1513-1521.

Brown, S. D., Twells, R. C., Hey, P. J., Cox, R. D., Levy, E. R., Soderman, A. R., Metzker, M. L., Caskey, C. T., Todd, J. A. and Hess, J. F. (1998). Isolation and characterization of LRP6, a novel member of the low density lipoprotein receptor gene family. *Biochem. Biophys. Res. Commun.* **248**, 879-888.

Bulman, M. P., Kusumi, K., Frayling, T. M., McKeown, C., Garrett, C., Lander, E. S., Krumlauf, R., Hattersley, A. T., Ellard, S. and Turnpenny, P. D. (2000). Mutations in the human delta homologue, DLL3, cause axial skeletal defects in spondylocostal dysostosis. *Nat. Genet.* **24**, 438-441.

Burgess, R., Cserjesi, P., Ligon, K. L. and Olson, E. N. (1995). Paraxis: a basic helix-loop-helix protein expressed in paraxial mesoderm and developing somites. *Dev. Biol.* **168**, 296-306.

Burgess, R., Rawls, A., Brown, D., Bradley, A. and Olson, E. N. (1996). Requirement of the paraxis gene for somite formation and musculoskeletal patterning. *Nature* **384**, 570-573.

Capdevila, J., Tabin, C. and Johnson, R. L. (1998). Control of dorsoventral somite patterning by Wnt-1 and beta-catenin. *Dev. Biol.* **193**, 182-194.

Correia, K. M. and Conlon, R. A. (2000). Surface ectoderm is necessary for the morphogenesis of somites. *Mech. Dev.* **91**, 19-30.

Evrard, Y. A., Lun, Y., Aulehla, A., Gan, L. and Johnson, R. L. (1998). lunatic fringe is an essential mediator of somite segmentation and patterning. *Nature* **394**, 377-381.

Fan, C. M., Lee, C. S. and Tessier-Lavigne, M. (1997). A role for WNT proteins in induction of dermomyotome. *Dev. Biol.* **191**, 160-165.

Fujino, T., Asaba, H., Kang, M. J., Ikeda, Y., Sone, H., Takada, S., Kim, D. H., Ioka, R. X., Ono, M., Tomoyori, H. et al. (2003). Low-density lipoprotein receptor-related protein 5 (LRP5) is essential for normal cholesterol metabolism and glucose-induced insulin secretion. *Proc. Natl. Acad. Sci. USA* **100**, 229-234.

Galceran, J., Farinas, I., Depew, M. J., Clevers, H. and Grosschedl, R. (1999). Wnt3a-/–like phenotype and limb deficiency in Lef1(–/–)Tcf1(–/–) mice. *Genes Dev.* **13**, 709-717.

Galceran, J., Hsu, S. C. and Grosschedl, R. (2001). Rescue of a Wnt mutation by an activated form of LEF-1: regulation of maintenance but not initiation of Brachyury expression. *Proc. Natl. Acad. Sci. USA* **98**, 8668-8673.

Galli, L. M., Willert, K., Nusse, R., Yablonka-Reuveni, Z., Nohno, T., Denetclaw, W. and Burrus, L. W. (2004). A proliferative role for Wnt-3a in chick somites. *Dev. Biol.* **269**, 489-504.

Gong, Y., Slee, R. B., Fukai, N., Rawadi, G., Roman-Roman, S., Reginato, A. M., Wang, H., Cundy, T., Glorieux, F. H., Lev, D. et al. (2001). LDL receptor-related protein 5 (LRP5) affects bone accrual and eye development. *Cell* **107**, 513-523.

Grüneberg, H. (1961). Genetical studies on the skeleton of the mouse. XXIX. Pudgy. *Genet. Res.* **2**, 384-393.

Hamblet, N. S., Lijam, N., Ruiz-Lozano, P., Wang, J., Yang, Y., Luo, Z., Mei, L., Chien, K. R., Sussman, D. J. and Wynshaw-Boris, A. (2002). Dishevelled 2 is essential for cardiac outflow tract development, somite segmentation and neural tube closure. *Development* **129**, 5827-5838.

He, X., Semenov, M., Tamai, K. and Zeng, X. (2004). LDL receptor-related proteins 5 and 6 in Wnt/beta-catenin signaling: Arrows point the way. *Development* **131**, 1663-1667.

Hey, P. J., Twells, R. C., Phillips, M. S., Nakagawa, Y., Brown, S. D., Kawaguchi, Y., Cox, R., Xie, G., Dugan, V., Hammond, H. et al. (1998). Cloning of a novel member of the low-density lipoprotein receptor family. *Gene* **216**, 103-111.

Hsu, S. C., Galceran, J. and Grosschedl, R. (1998). Modulation of transcriptional regulation by LEF-1 in response to Wnt-1 signaling and association with β-catenin. *Mol. Cell. Biol.* **18**, 4807-4818.

Jeon, H., Meng, W., Takagi, J., Eck, M. J., Springer, T. A. and Blacklow, S. C. (2001). Implications for familial hypercholesterolemia from the structure of the LDL receptor YWTD-EGF domain pair. *Nat. Struct. Biol.* 8, 499-504.

Johnson, J., Rhee, J., Parsons, S. M., Brown, D., Olson, E. N. and Rawls, A. (2001). The anterior/posterior polarity of somites is disrupted in paraxis-deficient mice. *Dev. Biol.* **229**, 176-187.

Kato, M., Patel, M. S., Levasseur, R., Lobov, I., Chang, B. H., Glass, D. A., 2nd, Hartmann, C., Li, L., Hwang, T. H., Brayton, C. F. et al. (2002). Cbfa1-independent decrease in osteoblast proliferation, osteopenia, and persistent embryonic eye vascularization in mice deficient in Lrp5, a Wnt coreceptor. *J. Cell Biol.* **157**, 303-314.

Kelly, O. G., Pinson, K. I. and Skarnes, W. C. (2004). The Wnt co-receptors Lrp5 and Lrp6 are essential for gastrulation in mice. *Development* **131**, 2803-2815.

Kessel, M., Balling, R. and Gruss, P. (1990). Variations of cervical vertebrae after expression of a Hox-1.1 transgene in mice. *Cell* **61**, 301-308.

Kokubu, C., Wilm, B., Kokubu, T., Wahl, M., Rodrigo, I., Sakai, N., Santagati, F., Hayashizaki, Y., Suzuki, M., Yamamura, K. et al. (2003). Undulated short-tail deletion mutation in the mouse Ablates Pax1 and leads to ectopic activation of neighboring Nkx2-2 in domains that normally express Pax1. *Genetics* **165**, 299-307.

Kraus, F., Haenig, B. and Kispert, A. (2001). Cloning and expression analysis of the mouse T-box gene Tbx18. *Mech. Dev.* **100**, 83-86.

Kuhlbrodt, K., Herbarth, B., Sock, E., Hermans-Borgmeyer, I. and Wegner, M. (1998). Sox10, a novel transcriptional modulator in glial cells. *J. Neurosci.* **18**, 237-250.

Kusumi, K., Sun, E. S., Kerrebrock, A. W., Bronson, R. T., Chi, D. C., Bulotsky, M. S., Spencer, J. B., Birren, B. W., Frankel, W. N. and Lander, E. S. (1998). The mouse pudgy mutation disrupts Delta homologue Dll3 and initiation of early somite boundaries. *Nat. Genet.* **19**, 274-278.

Leitges, M., Neidhardt, L., Haenig, B., Herrmann, B. G. and Kispert, A. (2000). The paired homeobox gene Uncx4.1 specifies pedicles, transverse processes and proximal ribs of the vertebral column. *Development* **127**, 2259-2267.

Little, R. D., Carulli, J. P., Del Mastro, R. G., Dupuis, J., Osborne, M., Folz, C., Manning, S. P., Swain, P. M., Zhao, S. C., Eustace, B. et al. (2002). A mutation in the LDL receptor-related protein 5 gene results in the autosomal dominant high-bone-mass trait. *Am. J. Hum. Genet.* **70**, 11-19.

Magoori, K., Kang, M. J., Ito, M. R., Kakuuchi, H., Ioka, R. X., Kamataki, A., Kim, D. H., Asaba, H., Iwasaki, S., Takei, Y. A. et al. (2003). Severe hypercholesterolemia, impaired fat tolerance, and advanced atherosclerosis in mice lacking both low density lipoprotein receptor-related protein 5 and apolipoprotein E. *J. Biol. Chem.* **278**, 11331-11336.

Mansouri, A., Yokota, Y., Wehr, R., Copeland, N. G., Jenkins, N. A. and Gruss, P. (1997). Paired-related murine homeobox gene expressed in the developing sclerotome, kidney, and nervous system. *Dev. Dyn.* **210**, 53-65.

Mao, B., Wu, W., Li, Y., Hoppe, D., Stannek, P., Glinka, A. and Niehrs, C. (2001a). LDL-receptor-related protein 6 is a receptor for Dickkopf proteins. *Nature* **411**, 321-325.

Mao, J., Wang, J., Liu, B., Pan, W., Farr, G. H., 3rd, Flynn, C., Yuan, H., Takada, S., Kimelman, D., Li, L. et al. (2001b). Low-density lipoprotein receptor-related protein-5 binds to Axin and regulates the canonical Wnt signaling pathway. *Mol. Cell* **7**, 801-809.

McEwen, D. G. and Peifer, M. (2001b). Wnt signaling: the naked truth? *Curr. Biol.* **11**, R524-R526.

Morgan, W. C. (1954). A new crooked tail mutation involving distinctive pleiotropism. *J. Genet.* **52**, 354-373.

Münsterberg, A. E., Kitajewski, J., Bumcrot, D. A., McMahon, A. P. and Lassar, A. B. (1995). Combinatorial signaling by Sonic hedgehog and Wnt family members induces myogenic bHLH gene expression in the somite. *Genes Dev.* **9**, 2911-2922.

Nykjaer, A. and Willnow, T. E. (2002). The low-density lipoprotein receptor gene family: a cellular Swiss army knife? *Trends Cell Biol.* **12**, 273-280.

Pinson, K. I., Brennan, J., Monkley, S., Avery, B. J. and Skarnes, W. C. (2000). An LDL-receptor-related protein mediates Wnt signalling in mice. *Nature* **407**, 535-538.

Pourquié, O. (2001). Vertebrate somitogenesis. *Annu. Rev. Cell Dev. Biol.* **17**, 311-350.

Pourquié, O. and Tam, P. P. (2001). A nomenclature for prospective somites and phases of cyclic gene expression in the presomitic mesoderm. *Dev. Cell* **1**, 619-620.

Saga, Y. and Takeda, H. (2001). The making of the somite: molecular events in vertebrate segmentation. *Nat. Rev. Genet.* **2**, 835-845.

Saga, Y., Hata, N., Koseki, H. and Taketo, M. M. (1997). Mesp2: a novel

mouse gene expressed in the presegmented mesoderm and essential for segmentation initiation. *Genes Dev.* **11**, 1827-1839.

Semenov, M. V., Tamai, K., Brott, B. K., Kuhl, M., Sokol, S. and He, X. (2001). Head inducer Dickkopf-1 is a ligand for Wnt coreceptor LRP6. *Curr. Biol.* **11**, 951-961.

Sosic, D., Brand-Saberi, B., Schmidt, C., Christ, B. and Olson, E. N. (1997). Regulation of paraxis expression and somite formation by ectoderm- and neural tube-derived signals. *Dev. Biol.* **185**, 229-243.

Strickland, D. K., Gonias, S. L. and Argraves, W. S. (2002). Diverse roles for the LDL receptor family. *Trends Endocrinol. Metab.* **13**, 66-74.

Takada, S., Stark, K. L., Shea, M. J., Vassileva, G., McMahon, J. A. and McMahon, A. P. (1994). Wnt-3a regulates somite and tailbud formation in the mouse embryo. *Genes Dev.* **8**, 174-189.

Takagi, J., Yang, Y., Liu, J., Wang, J. and Springer T. A. (2003). Complex between nidogen and laminin fragments reveals a paradigmatic b-propeller interface. *Nature* **424**, 969-974.

Takahashi, Y., Koizumi, K., Takagi, A., Kitajima, S., Inoue, T., Koseki, H. and Saga, Y. (2000). Mesp2 initiates somite segmentation through the Notch signalling pathway. *Nat. Genet.* **25**, 390-396.

Tamai, K., Semenov, M., Kato, Y., Spokony, R., Liu, C., Katsuyama, Y., Hess, F., Saint-Jeannet, J. P. and He, X. (2000). LDL-receptor-related proteins in Wnt signal transduction. *Nature* **407**, 530-535.

Theiler, K. (1968). Das Wirbel-Rippen-Syndrom. *Schweiz. Med. Wochenschr.* **98**, 907-908.

Theiler, K. (1988). Vertebral malformations. *Adv. Anat. Embryol. Cell Biol.* **112**, 1-99.

Theiler, K. and Glücksohn-Wälsch, S. (1956). The morphological effects and the development of the fused mutation in the mouse. *Anat. Rec.* **125**, 83-103.

Theiler, K. and Stevens, L. C. (1960). The development of rib fusions, a mutation in the house mouse. *Am. J. Anat.* **106**, 171-183.

Theiler, K. and Varnum, D. S. (1985). Development of rib-vertebrae: a new mutation in the house mouse with accessory caudal duplications. *Anat. Embryol.* **173**, 111-116.

Theiler, K., Varnum, D. S., Southard, J. L. and Stevens, L. C. (1975). Malformed vertebrae: a new mutant with the 'wirbel-rippen syndrom' in the mouse. *Anat. Embryol.* **147**, 161-166.

Theiler, K., Varnum, D. and Stevens, L. C. (1974). Development of rachiterata, a mutation in the house mouse with 6 cervical vertebrae. *Z. Anat. Entwicklungsgesch.* **145**, 75-80.

Wagner, J., Schmidt, C., Nikowits, W., Jr and Christ, B. (2000). Compartmentalization of the somite and myogenesis in chick embryos are influenced by wnt expression. *Dev. Biol.* **228**, 86-94.

Wehrli, M., Dougan, S. T., Caldwell, K., O'Keefe, L., Schwartz, S., Vaizel-Ohayon, D., Schejter, E., Tomlinson, A. and DiNardo, S. (2000). arrow encodes an LDL-receptor-related protein essential for Wingless signalling. *Nature* **407**, 527-530.

Yashiro, K., Zhao, X., Uehara, M., Yamashita, K., Nishijima, M., Nishino, J., Saijoh, Y., Sakai, Y. and Hamada, H. (2004). Regulation of retinoic acid distribution is required for proximodistal patterning and outgrowth of the developing mouse limb. *Dev. Cell* **6**, 411-422.

Yoshikawa, Y., Fujimori, T., McMahon, A. P. and Takada, S. (1997). Evidence that absence of Wnt-3a signaling promotes neuralization instead of paraxial mesoderm development in the mouse. *Dev. Biol.* **183**, 234-242.

Zeng, L., Fagotto, F., Zhang, T., Hsu, W., Vasicek, T. J., Perry, W. L., 3rd, Lee, J. J., Tilghman, S. M., Gumbiner, B. M. and Costantini, F. (1997). The mouse Fused locus encodes Axin, an inhibitor of the Wnt signaling pathway that regulates embryonic axis formation. *Cell* **90**, 181-192.

Zhang, N. and Gridley, T. (1998). Defects in somite formation in lunatic fringe-deficient mice. *Nature* **394**, 374-377.

Zorn, A. M. (2001). Wnt signalling: antagonistic Dickkopfs. *Curr. Biol.* **11**, R592-R595.